A Dipole Pattern of Summertime Rainfall across the Indian Subcontinent and the Tibetan Plateau

XINGWEN JIANG

Institute of Plateau Meteorology, China Meteorological Administration, and Heavy Rain and Drought–Flood Disasters in Plateau and Basin Key Laboratory of Sichuan Province, Chengdu, Sichuan, China

MINGFANG TING

Lamont-Doherty Earth Observatory, Columbia University, Palisades, New York

(Manuscript received 27 December 2016, in final form 31 August 2017)

ABSTRACT

The Tibetan Plateau (TP) has long been regarded as a key driver for the formation and variations of the Indian summer monsoon (ISM). Recent studies, however, have indicated that the ISM also exerts a considerable impact on rainfall variations in the TP, suggesting that the ISM and the TP should be considered as an interactive system. From this perspective, the covariability of the July–August mean rainfall across the Indian subcontinent (IS) and the TP is investigated. It is found that the interannual variation of IS and TP rainfall exhibits a dipole pattern in which rainfall in the central and northern IS tends to be out of phase with that in the southeastern TP. This dipole pattern is associated with significant anomalies in rainfall, atmospheric circulation, and water vapor transport over the Asian continent and nearby oceans. Rainfall anomalies and the associated latent heating in the central and northern IS tend to induce changes in regional circulation that suppress rainfall in the southeastern TP and vice versa. Furthermore, the sea surface temperature anomalies in the tropical southeastern Indian Ocean can trigger the dipole rainfall pattern by suppressing convection over the central IS and the northern Bay of Bengal, which further induces anomalous anticyclonic circulation to the south of TP that favors more rainfall in the southeastern TP by transporting more water vapor to the region. The dipole pattern is also linked to the Silk Road wave train via its link to rainfall over the northwestern IS.

1. Introduction

Interannual variations of summertime rainfall in the Indian subcontinent (IS) brought by the Indian monsoon has a significant impact on local agriculture and the environment (e.g., Gadgil and Rupa Kumar 2006). Variations of the Indian monsoon also affect climate beyond the IS by altering atmospheric circulation due to associated latent heating (Hu et al. 2005; Ding and Wang 2005; Wei et al. 2014). Both external forcing (e.g., sea surface temperature anomalies in various ocean basins) and internal atmospheric processes (e.g., atmospheric intraseasonal variations) contribute to interannual variations of the Indian monsoon rainfall (e.g., Kumar et al. 1999; Goswami and Ajayamohan 2001; Gadgil 2003). Although great efforts have been devoted to the understanding of interannual variations of the Indian monsoon, the prediction skill for Indian monsoon rainfall remains low (Wang et al. 2015).

The Tibetan Plateau (TP), located to the northeast of the IS, has long been recognized as an important driver for the formation and variations of the Asian monsoon through both mechanical and thermal forcings (e.g., Yanai et al. 1992; Li and Yanai 1996; Wu et al. 2007; Z. Wu et al. 2012), although the relative contribution of the thermal and mechanical effects may be debated (Boos and Kuang 2010; G. Wu et al. 2012). The controversy is at least partly due to the relatively poor representation of the climate models' simulation around the TP (Qiu 2013). It should be noted that this controversy was focused on the effects of the TP on the formation of theIndian summer monsoon

Corresponding author: Dr. Xingwen Jiang, xingwen.jiang@yahoo.com

DOI: 10.1175/JCLI-D-16-0914.1

rather than its variations. Some studies indicated that thermal condition over the TP is linked to the Indian summer monsoon on an interannual time scale.

Using reanalysis data, the study of Rajagopalan and Molnar (2013) indicated that the thermal condition, represented by moist static energy, over the western TP correlates significantly with the Indian monsoon rainfall during the onset and decay periods, but not during the peak monsoon season. On the other hand, Bansod et al. (2003) reported that the January thermal condition, measured by surface air temperature over the northeastern TP, is negatively correlated with the following summer Indian monsoon rainfall along the monsoon trough region. These studies indicate that there are temporal and spatial dependencies in the relationship between the Indian monsoon rainfall and the TP thermal conditions. The dominant component of the summertime atmospheric heat source over TP is different between west and east for both climatology and interannual variability (Yang et al. 2011; Jiang et al. 2016). While Rajagopalan and Molnar (2013) reported that there is no significant correlation between thermal condition over the western TP and IS rainfall during peak monsoon season, the relationship between the thermal condition over other parts of the TP and IS rainfall during the peak monsoon season remains unclear.

G. Wu et al. (2012) reported that sensible heating over the TP, especially along the southern slopes, is important for driving the tropical water vapor northward to the TP and resultant rainfall there; condensation heating of the rainfall acts as a positive feedback on the circulation and thus amplifies the effect of sensible heat. Climatologically, the atmospheric heat source is dominated by sensible heat over the western TP but latent heat over the central and eastern TP (Zhao and Chen 2001; Yang et al. 2011). Interannual variations of the summertime atmospheric heat source over the eastern and central TP are also dominated by latent heating (Jiang et al. 2016). Therefore, the effect of latent heating (rainfall) may be of primary importance as the heat source that drives regional circulation change on interannual time scales.

Most previous studies focused on the impact of the TP on the Indian monsoon, but recent studies have indicated that the Indian monsoon can also affect summertime rainfall in the TP on a wide range of time scales (Xu et al. 2008; Yao et al. 2013; Jiang et al. 2016) while being modulated by atmospheric processes over the midlatitudes (Liu and Yin 2001). The Indian summer monsoon (ISM) affects rainfall in the southern TP by modulating incoming water vapor transport (Chen et al. 2012; Feng and Zhou 2012; Dong et al. 2016) and land–atmosphere energy exchange over the TP (Zhou et al. 2015). Thus, the TP and the Indian monsoon should be considered as an interactive system.

We focus in this study on the covariability of rainfall in the TP and IS and its possible cause. In the rest of this paper, the data, methods, and model used are described in section 2. A dipole pattern of rainfall across the IS and TP and related atmospheric circulation characteristics are presented in section 3. Possible interactions of rainfall anomalies between the IS and the TP, and the role of tropical sea surface temperature (SST) in the dipole rainfall pattern, are discussed in sections 4 and 5, respectively. Possible relationships among the dipole pattern, the Silk Road wave train, and ENSO are discussed in section 6. Finally, a summary is provided in section 7.

2. Data, methods, and model

a. Data

In this study, we use rainfall data from Asian Precipitation—Highly Resolved Observational Data Integration toward Evaluation of Water Resources (APHRODITE) to illustrate the variation of rainfall over the IS and the TP. APHRODITE is a compilation of rain gauge data from weather stations. Because of the emphasis on Asian rainfall in this study, a subset of APHRODITE covering mostly Asian land (15°S–55°N, 60°–150°E), is used (APHRO_MA_V1101). The product includes daily rainfall from 1951 to 2007, with a spatial resolution of 0.5° in both latitude and longitude. The amount of rainfall shows a large horizontal variation between the main body of the TP and the surrounding areas due to the sharp topography gradients. The APHRODITE rainfall data have an advantage in this region because of improvements in the high-density coverage of rain gauge stations and interpolation/extrapolation algorithms (Yatagai et al. 2012).

The datasets used in this study also include the National Centers for Environmental Prediction (NCEP)–National Center for Atmospheric Research (NCAR) reanalysis from 1951 to 2015 (Kalnay et al. 1996), monthly mean SST from the HadISST dataset from 1951 to 2015 with a horizontal resolution of 1° in both latitude and longitude (Rayner et al. 2003), and National Oceanic and Atmospheric Administration interpolated outgoing longwave radiation (OLR) from 1974 to 2015 (Liebmann and Smith 1996). The high-vertical-resolution ERA-Interim from 1979 to 2015 (Dee et al. 2011) is used to drive a nonlinear baroclinic model. To verify the results obtained from the APHRODITE rainfall in areas with few rain gauge stations and reflect convection over tropical oceans, we also use monthly mean rainfall from the Global Precipitation Climatology

Project (GPCP) monthly rainfall analysis dataset, version 2.2, from 1979 to 2015 (Adler et al. 2003) in this study.

b. Methods

To investigate the different roles of SSTs in the tropical Indian Ocean (IO) and the tropical Pacific on rainfall over the IS and the TP, partial correlations (e.g., Behera and Yamagata 2003) and partial regression are used in this study. The partial correlation coefficient between two variables A1 and A2, after removing the influence of variable A3, is expressed as $r_{12,3} = (r_{12} - r_{13}r_{23})[(1 - r_{13}^2)(1 - r_{23}^2)]^{-1/2}$ and r_{12} is the correlation between A1 and A2 (likewise, r_{13} is the correlation between A1 and A3, and r_{23} between A2 and A3).

The partial regression is expressed as $Y = b_0 + b_1X_1 + b_2X_2$, where b_0 represents the predicted value of Y when the other two variables are equal to zero, and b_1 and b_2 are the partial regression coefficients between Y and X_1 and between Y and X_2, respectively. In this study, the independent variables X_1 and X_2 are normalized SST in the tropical southeastern Indian Ocean and the tropical Pacific, respectively; the dependent variable Y is either wind or rainfall.

To highlight the interannual time scale variations, a 9-yr Gaussian filter was first applied to the time series for each variable to remove the interdecadal fluctuations. All statistical significance tests for correlations and regressions are performed using the two-tailed Student's t test.

The vertically integrated moisture flux was computed as follows:

$$\mathbf{Q} = \frac{1}{g}\int_{300}^{p_s} q\mathbf{V}\,dp,$$

where q is the specific humidity, $\mathbf{V}$ the horizontal wind vector, p the air pressure, p_s the surface pressure, and g the gravitational constant.

c. Model

To investigate the impact of diabatic heating associated with the rainfall anomaly on the regional circulation, a nonlinear baroclinic model developed by Ting and Yu (1998) is employed in this study. This model is a nonlinear, dry, time-dependent baroclinic model with 24 sigma levels in the vertical and spectral R30 horizontal resolution. This model was originally designed to solve the nonlinear primitive equations for deviations from a prescribed zonal-mean basic state in response to zonally asymmetric imposed forcings. In this study, we use it to simulate atmospheric response to heating in a specific region with a climatological zonally varying basic state taken from the ERA-Interim. The dissipations employed in the model include Rayleigh friction, Newtonian cooling, and biharmonic diffusion (coefficient of $1 \times 10^{17}\,\mathrm{m^4\,s^{-1}}$). The coefficients of Rayleigh friction and Newtonian cooling are the same, with time scales of 0.3, 0.5, 1.0, and 8.0 days in the lowest four levels, and 15 days in the other levels. The time integration is performed for 50 days. The model solution approaches a steady state after about 15 days and the average for the last 20 days are shown in this study.

The idealized heating related to rainfall anomaly is prescribed as $Q = AV(\sigma)H(\lambda, \phi)$, where A is the amplitude and chosen to be $1°\mathrm{C\,day^{-1}}$ in this study, and $H(\lambda, \phi)$ is set to 1 in a specific region and 0 outside the region. The vertical heating profile takes the form $V(\sigma) = \exp[-20(\sigma - \sigma_c)^2]$, which has a maximum at $\sigma = \sigma_c$ and reduces to zero as σ increases or decreases from σ_c. The simulation results are not sensitive to the vertical decay rate, which is chosen to be 20 in this study. Because of the different altitudes of the IS and the TP, σ_c is chosen to be 0.5 and 0.65 for the IS and the TP, respectively. Responses of atmospheric circulation in the lower and upper troposphere are not sensitive to the precise location of σ_c.

3. A dipole pattern of interannual variation of rainfall across the IS and TP

Figure 1a shows the mean (shading) and variance (contours) of July–August rainfall over the IS and TP. A comparison of patterns between the mean and the variance of rainfall indicates that regions with high mean rainfall coincide well with regions of large rainfall variance. There are two rainfall maxima in the IS: one located along the southwestern coast and the other in the eastern-central India. The former is caused by interaction of the southwestern monsoon flows and orography parallel to the coast; the latter is often called the core monsoon zone (Gadgil 2003). The variation of rainfall in the core monsoon zone is highly correlated with the variation of all-India summer rainfall, which is widely used to measure the variation of the ISM (Gadgil 2003). Thus, rainfall variation in this region is the focus of many ISM studies. As for rainfall in the TP, a maximum rainfall band is located at the southern slopes. The southeast of the main body of TP receives a considerable amount of rainfall (above $3\,\mathrm{mm\,day^{-1}}$) while the northwest is relatively dry (below $1\,\mathrm{mm\,day^{-1}}$). The latent heating associated with the large amount of rainfall in both the IS and the TP plays a vital role in driving the ISM circulation (G. Wu et al. 2012; Boos and Kuang 2013).

To reveal the possible relationship of interannual variation of rainfall between the IS and TP, an empirical

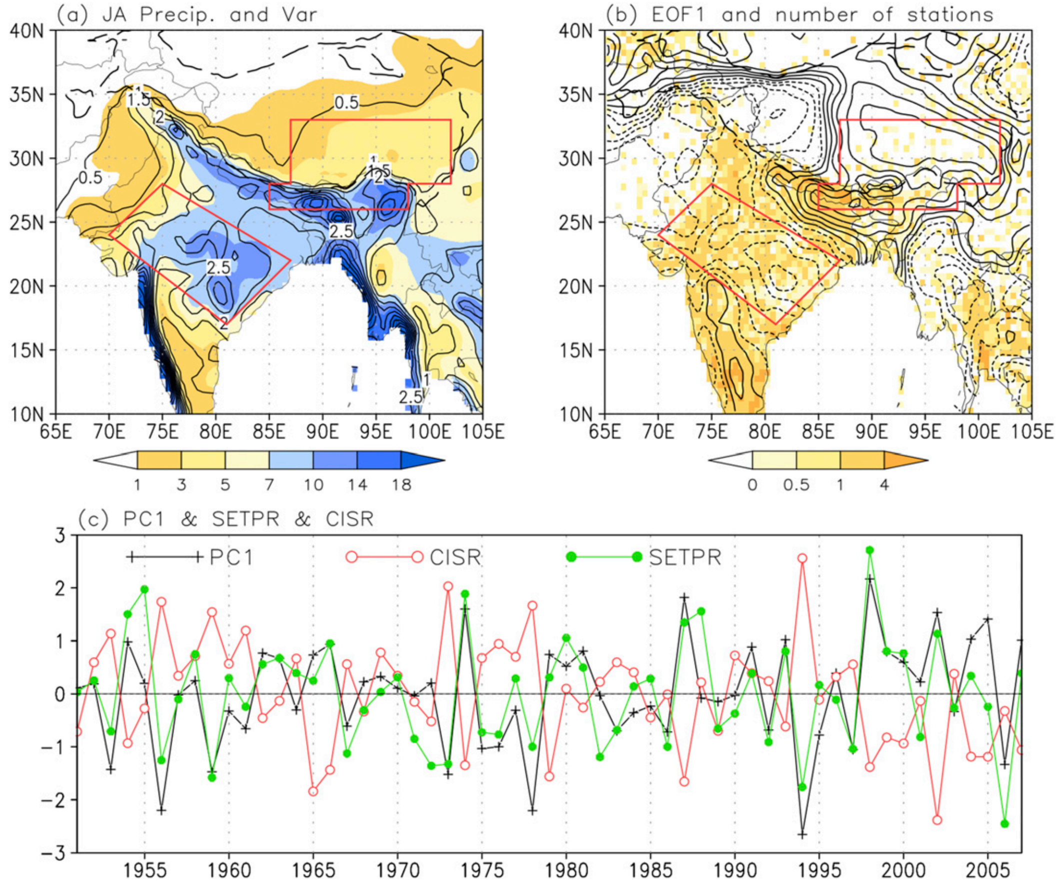

FIG. 1. (a) Mean (shading) and variance (contours) of July–August APHRODITE rainfall from 1951 to 2007 (mm day^{-1}). (b) Spatial pattern of the first mode of an EOF analysis applied to temporal correlation matrix of July–August rainfall (contours; contour interval is 0.5; dashed contours for negative values and solid contours for positive values) and mean number of rain gauge stations (shading). (c) Principal component (black curve with plus symbols) corresponding to spatial pattern in (b) and time series of normalized regional averaged rainfall in the southeastern TP (red curve with open circles) and the central IS (green curve with filled circles), which are outlined by the red boxes in (a) and (b).

orthogonal function (EOF) analysis is applied to the temporal correlation matrix of July–August rainfall. The first mode accounts for 16.8% of the total variance. Figure 1b presents the spatial pattern of the first mode, which shows a dipole pattern of rainfall anomalies, with negative values over the central and northern IS and the western TP, and positive values in the southeastern TP (SETP), including the main body and the southern slopes. Rainfall over the core monsoon region varies out of phase with rainfall over southern India, which is similar to the second EOF mode of year-to-year variability of Indian summer rainfall (Mishra et al. 2012). The spatial pattern of first EOF mode suggests that the ISM rainfall varies out of phase with rainfall in the SETP and in phase with rainfall in the western TP. It should be noted that there are very few rain gauge stations in the western TP and Afghanistan (shading in Fig. 1b), so rainfall data there may not be reliable. Therefore, we choose not to focus our attention on that region in this study. The dipole rainfall pattern does not change when the EOF analysis is applied to a larger domain or only to grids with rain gauge observations. In fact, a similar pattern can be seen when EOF analysis is applied to the entire monsoon region (15°S–55°N, 60°–150°E; Day et al. 2015). This dipole pattern is also reproduced when the EOF analysis is applied to the GPCP rainfall data from 1979 to 2015 (figure not shown). Following Wallace and Gutzler (1981), we also compute the correlations of rainfall over each grid point with rainfall over the rest of the grids (figures not shown). The correlation maps confirm a significant out-of-phase variation of rainfall between the two regions as suggested by the first mode.

To further illustrate the variation of rainfall in the IS and the TP, as well as their out-of-phase relationship, we constructed two rainfall indices by averaging the July–August rainfall over the central IS region (CISR) and

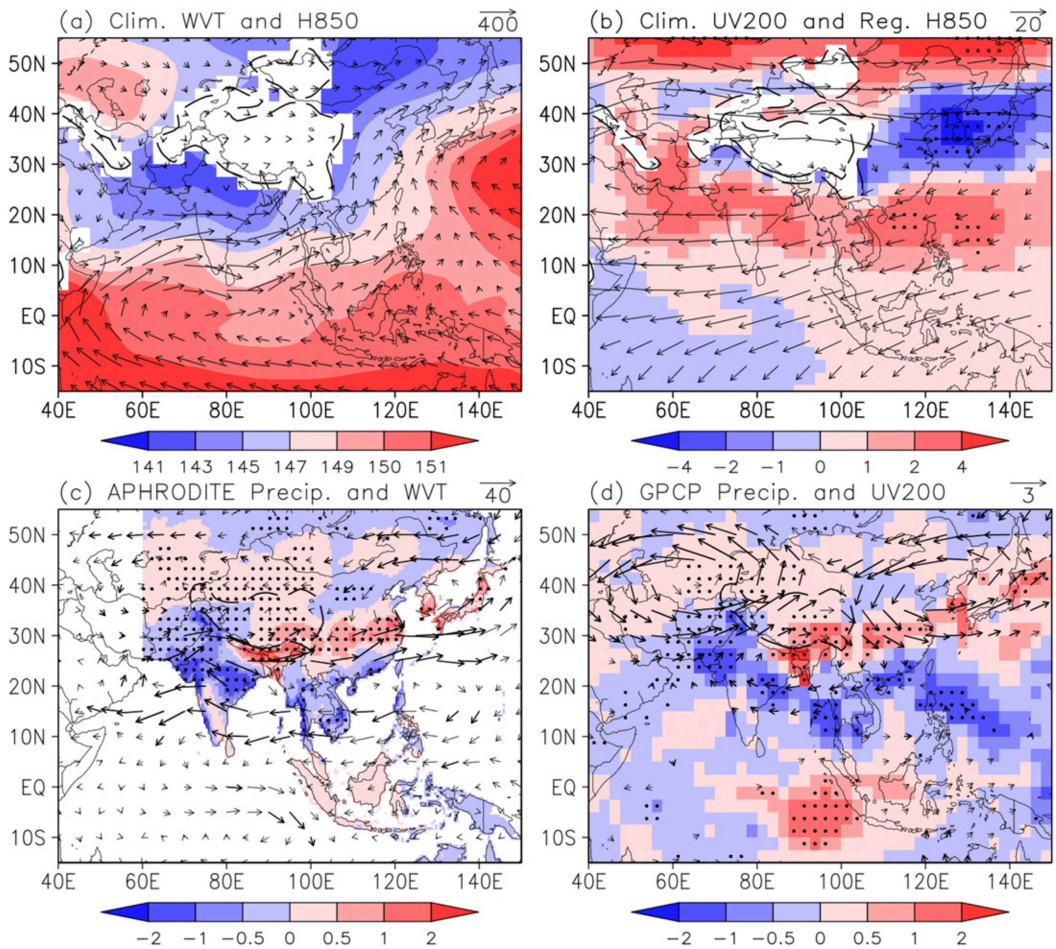

FIG. 2. (a) Climatological July–August 850-hPa geopotential height [geopotential dam (gpdam); contours] and vertically integrated WVT (kg $m^{-1} s^{-1}$; vectors). (b) Climatological July–August 200-hPa winds (m s^{-1}; vectors) and pattern of regression of 850-hPa geopotential height (10^1 gpdam; contours) on the PC1. (c) Patterns of regression of APHRODITE rainfall (mm day^{-1}; shading) and vertically integrated WVT (kg $m^{-1} s^{-1}$; vectors) on PC1. (d) Patterns of regression of GPCP rainfall (mm day^{-1}; shading, 1979–2007) and 200-hPa winds (m s^{-1}; vectors) on the PC1. Stippling indicates the value of the shading exceeding 95% confidence level in (b)–(d); thick arrows indicate values exceeding 95% confidence level in either the zonal or the meridional component in (b)–(d); the black dashed lines denote a topographic height of 1500 m in (a)–(c) and 3000 m in (d). Winds at 850 (200) hPa with speed lower than 0.1 (0.4) m s^{-1} are omitted.

the southeastern TP region (SETPR) (the two red boxes in Figs. 1a,b). The temporal variations of SETPR and CISR, as well as the principal component of the first EOF mode (PC1) are shown in Fig. 1c. Consistent with the first EOF mode, the CISR and the SETPR vary out of phase, with a significant correlation coefficient of −0.57. The correlation coefficients between the CISR and the SETPR are −0.12, −0.71, −0.59, and −0.31 for June, July, August, and September, respectively. The high negative correlations for July and August motivated our focus on July–August mean rainfall in this study.

Figure 2a shows the climatological July–August 850-hPa geopotential height (contours) and the vertically integrated water vapor transport (WVT; vectors). In the lower troposphere, the oceanic regions are dominated by high pressure while the Asian land region is controlled by a low pressure belt centered over the IS. Water vapor entering the SETP is transported by the southwesterly monsoon flow. It is worth noting that while westerly WVT prevails over the southern IS, there is no apparent dominant direction of WVT over northern IS, including the core monsoon region. In the upper troposphere, a large anticyclone is noticed, with a westerly jet stream in the midlatitudes and an easterly jet stream in the tropics (Fig. 2b).

The regression patterns of the atmospheric circulation and rainfall onto PC1 (Figs. 2b–d) indicate that the 850-hPa geopotential height increases both in the tropics and north of 50°N but decreases in subtropical East Asia when PC1 is positive (Fig. 2b). In the upper troposphere, a positive PC1 is associated with an anomalous anticyclone to the south of TP and two anomalous cyclones at midlatitudes (Fig. 2d), with one located in central Asia and the other in northeastern Asia.

The pattern of WVT anomalies related to PC1 is similar to that of 850-hPa wind anomalies over South and East Asia (Figs. 2b and 2c, respectively), suggesting that the WVT anomalies in these regions are dominated by low-level wind anomalies. In South Asia, a positive PC1 is associated with an anomalous easterly WVT south of 20°N but an anomalous westerly WVT to the north. The anomalous westerly WVT over the northern IS significantly weakens the climatological WVT from the Bay of Bengal to the central and northern IS, while anomalous southwesterlies enhance the water vapor transport to the SETP. The pattern of regression of rainfall from both APHRODITE and GPCP onto PC1 (Figs. 2c and 2d, respectively) is consistent with that of the water vapor transport anomalies, with reduced rainfall in the central and northern IS and enhanced rainfall in the southeastern TP when PC1 is positive. The two different rainfall datasets show remarkably consistent patterns despite the differences in the source data (with satellite observations incorporated in GPCP) and the analysis period. Furthermore, the dipole rainfall pattern in TP and the IS is not limited to these two local regions, but has anomalies extending to the Philippine Sea and Japan. Significant increases in rainfall can also be found in central Asia and the tropical southeastern Indian Ocean when PC1 is positive (Fig. 2d).

Comparisons among anomalous rainfall, WVT, and 850-hPa geopotential height related to PC1 indicate that the increase in geopotential height suppresses rainfall from the IS to the Philippine Sea by weakening the climatological monsoon trough. The anomalous anticyclonic WVT in IS caused anomalous divergence of water vapor flux (figures not shown), favoring below-normal rainfall there. On the other hand, the increase in rainfall from the southeastern TP to Japan is accompanied by the convergence of water vapor flux (figures not shown). The upper-tropospheric circulation anomalies feature two cyclones along the westerly jet stream in the midlatitudes with centers at 90° and 120°E, respectively, which resembles the so-called Silk Road wave train (e.g., Kosaka et al. 2012). As will be shown in section 6, the upper-tropospheric circulation mainly interacts with rainfall anomaly in the northwestern IS.

The above analyses provide an overall picture of the dipole rainfall pattern and the related atmospheric anomalies. The question is what are the relevant processes that cause the dipole rainfall pattern. There are two possible ways by which the dipole rainfall pattern may be formed. One possibility is that the rainfall anomaly in one location may cause an anomaly in the other location by altering the regional atmospheric dynamic and thermodynamic processes. The other possibility is that some remote factors may exert an opposite effect on rainfall in the two poles. These two possibilities are separately examined in the following two sections.

4. Possible interactions of rainfall anomalies between the IS and the TP

In this section, we examine the possibility that rainfall anomalies in the SETP may lead to rainfall anomaly in the central and northern IS, and vice versa. Figure 3 illustrates circulation and rainfall anomalies related to the SETPR and the CISR, respectively. The patterns of anomalous rainfall and winds related to the SETPR are generally opposite to those related to the CISR. However, there are some interesting differences in the relative amplitude of the anomalies at different locations. For example, the SETPR is associated with more significant rainfall and wind anomalies over Southeast Asia (Fig. 3a) while the CISR is associated with more significant anomalies over the Indian Ocean (Fig. 3c). Both are associated with significant rainfall anomalies in the tropical eastern Indian Ocean (shading in Figs. 3b,d) with opposite sign. It also can be seen that the two 200-hPa anomalous cyclones associated with PC1 in Fig. 2d are more related to the CISR than the SETPR. The significant correlation of rainfall between the TP and western Maritime Continent (Fig. 3a) is consistent with that reported by Jiang et al. (2016). They found that the enhanced convection over the western Maritime Continent can induce rainfall increases over the SETP.

To directly address the role of atmospheric latent heating over the TP and IS in driving the regional circulation, we use a dynamical model, the nonlinear baroclinic model as described in the method section, to simulate the circulation response to prescribed latent heating associated with rainfall anomalies over the SETP and IS. Figure 4 shows the baroclinic model response of low-level (0.87 sigma level) and upper-level (0.23 sigma level) winds and midlevel (0.37 sigma level) pressure vertical velocity to the diabatic heating (gray shading) over the SETP and the IS, respectively. The response to the heating over SETP is dominated by a cyclonic circulation around the TP in the lower troposphere and a large anticyclone in the upper troposphere, showing a baroclinic response. The low-level westerlies to the south of TP are consistent with below-normal rainfall in the northern IS as above-normal rainfall in this region is associated with anomalous easterlies (e.g.,

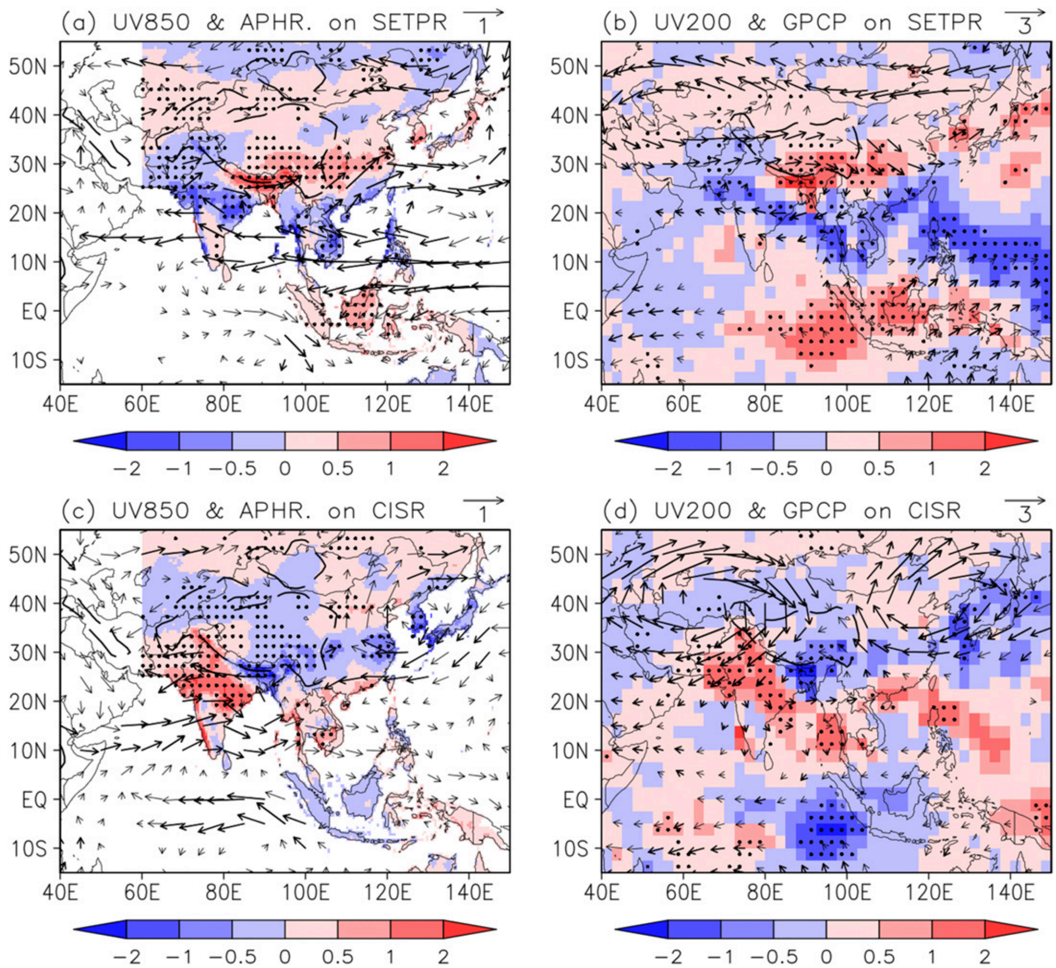

FIG. 3. (a) Patterns of regression of 850-hPa winds (m s^{-1}; vectors) and APHRODITE rainfall (mm day^{-1}; shading) on SETPR. (b) Patterns of regression of 200-hPa winds (m s^{-1}; vectors) and GPCP rainfall (mm day^{-1}; shading, 1979–2007) on the SETPR. (c),(d) As in (a),(b), but the SETPR is replaced by CISR. Stippling indicates the value of the shading exceeding 95% confidence level; thick arrows indicate values exceeding 95% confidence level in either the zonal or the meridional component; the black dashed lines denote the topographic height of 1500 m in (a) and (c) and 3000 m in (b) and (d). Winds at 850 (200) hPa with speed lower than 0.1 (0.4) m s^{-1} are omitted.

Fig. 3c). Furthermore, the SETP heating-induced upper-tropospheric divergent flow converges over the northwestern IS and western TP, resulting in descending motions there in the upper troposphere (Fig. 4b). Thus, the simulated response of regional circulation to heating over SETP indicates that it may cause below-normal rainfall over the northern IS. Results from a general circulation model and a high-resolution regional model also indicate that enhanced rainfall in the SETP caused by local surface sensible heating is associated with significantly reduced rainfall in the northern IS, especially the northwestern IS [see Fig. 3b in G. Wu et al. (2012) and Fig. 4f in Wang et al. (2016)].

In the lower troposphere, the heating over the central and northern IS excites cyclonic circulation to the northwest. In the upper troposphere, it induces a large anticyclone to the west and a weaker one to the northeast of the TP (Fig. 4c). While the lower-tropospheric circulation does not exert an apparent impact on the westerly flux of water vapor entering the TP, the heating causes significant descending motion over the SETP (Fig. 4d). Thus, the enhanced rainfall in the central and northern IS can suppress rainfall over the SETP by inducing upper-tropospheric descending motion.

The diabatic heating over the SETP excites an upper-tropospheric anticyclone to the west of TP in the simulation but the enhanced rainfall over the SETP is associated with an upper-tropospheric cyclone to the northwest of the TP in the observation (Figs. 3b and 4b). On the other hand, the diabatic heating over the central

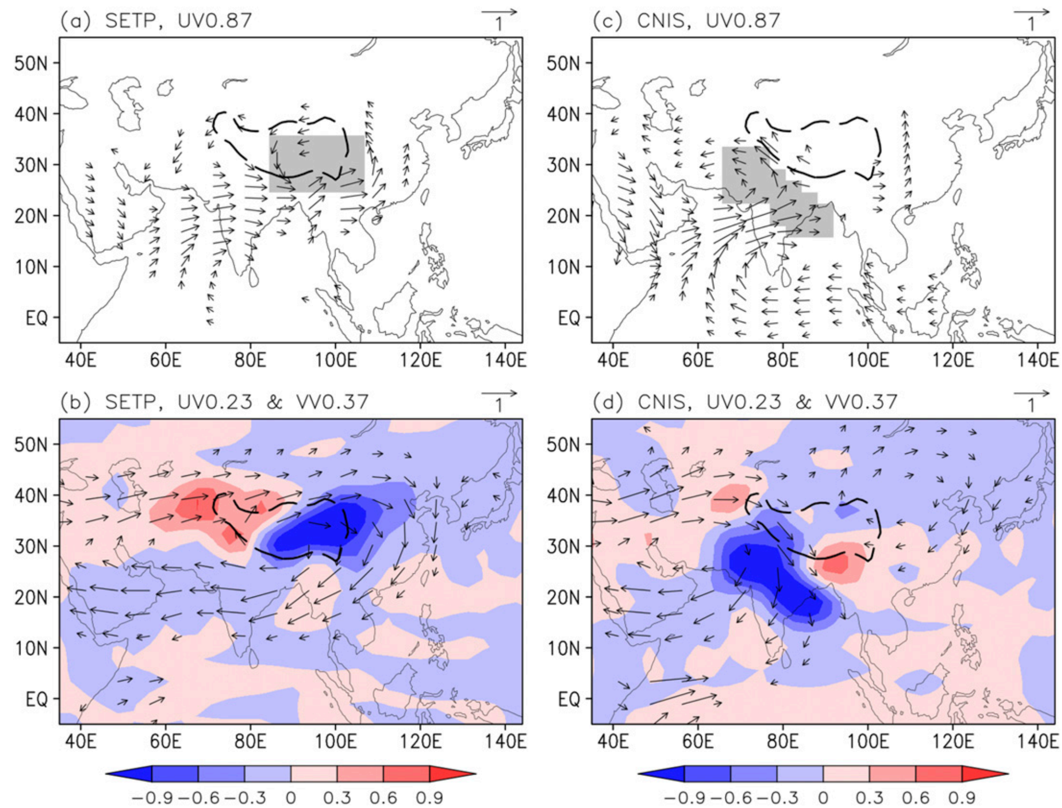

FIG. 4. Patterns of simulated horizontal wind ($m\,s^{-1}$; vectors) on (a) the 0.87 and (b) the 0.23 sigma level. Note that (b) also shows pressure vertical velocity on the 0.37 sigma level ($10^{-6}\,s^{-1}$; shading) by the nonlinear baroclinic model as a response to the heating over the SETP denoted by the gray shading. (c),(d) As in (a),(b), but the heating is over the central and northern IS as denoted by gray shading in (c). Winds with speed lower than $0.2\,m\,s^{-1}$ are omitted.

and northern IS excites an anticyclone to the west of the TP, consistent with the observation (Figs. 3d and 4d), and the simulated response to the diabatic cooling over the central and northern IS resembles the response to the diabatic heating with opposite sign (figures not shown). Thus, the upper-tropospheric winds associated with PC1 may be mostly caused by the diabatic cooling over the central and northern IS. Previous diagnostic study based on observation data also showed that the Indian monsoon rainfall anomaly contributes to the two anomalous cyclones in the midlatitudes (Ding and Wang 2005). The relationship between the upper-tropospheric circulation and rainfall over the IS will be further discussed in section 6.

The simulated anticyclone to the west of the heating over the central and northern IS extends more westward compared to the observation, while the simulated anticyclone to the northeast of the TP is weaker than the observation (Figs. 3d and 4d). This difference implies that rainfall anomalies in the SETP may also contribute to the anomalous upper-tropospheric winds pattern. We conducted two more experiments with prescribed heating over both the central and northern IS but cooling over the entire SETP or confined to the southeastern edge of the TP in the baroclinic model. The responses of the upper-tropospheric winds are presented in Fig. 5. There is a strong cyclone over the TP and a weak anticyclone over northeastern Asia when the cooling is over the entire southeastern TP (Fig. 5a). However, when the cooling is confined to the southeastern edge of the TP, there is a cyclone over the TP, and two anticyclones to the west of the heating and over northern China, respectively. Comparison between Figs. 5 and 4 indicates that the cooling over the SETP weakens the anticyclone to the east of the heating but shifts the anticyclone over northern China eastward.

The above analyses indicate that rainfall anomaly in the central and northern IS can cause an opposite rainfall anomaly over the SETP. However, the diabatic heating over the SETP mainly suppresses rainfall over the northern IS. We will show that southeastern Indian Ocean SST anomalies can cause opposite rainfall

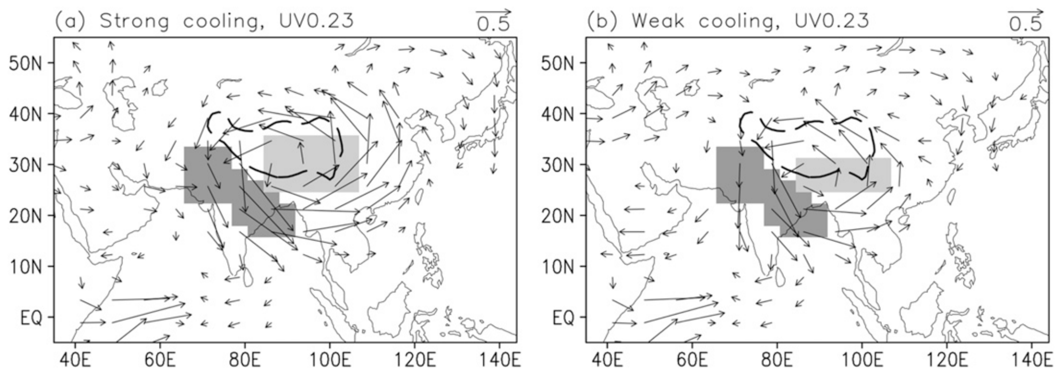

FIG. 5. Patterns of simulated horizontal wind (m s^{-1}; vectors) on the 0.23 sigma level by the nonlinear baroclinic model as a response to the heating (denoted by dark gray shading) over the central and northern IS but the cooling (denoted by light gray shading) (a) over the SETP or (b) confined to the southeastern edge of the TP. Winds with speed lower than 0.1 m s^{-1} are omitted.

anomalies between the central IS and SETP in the following section.

5. Relationships of the dipole rainfall pattern with sea surface temperature

Many previous studies reported that both El Niño–Southern Oscillation (ENSO) and the Indian Ocean dipole exert a significant impact on rainfall in the IS (e.g., Kumar et al. 1999, 2006; Ashok et al. 2001), whereas few studies focused on the relationship of summer rainfall over the SETP with SST. Figure 6 presents the regression coefficients of SST and OLR to PC1. It can be seen that a positive PC1 (more rainfall in southeastern TP and less rain in central IS) is associated with warmer than usual SST in the Arabian Sea, Bay of Bengal, and the tropical eastern Indian Ocean. There are also weak positive SST anomalies in the tropical central and eastern Pacific associated with positive PC1. It is worth noting that although ENSO is significantly correlated with the all-India rainfall, the PC1-related SST anomalies only show a weak warming in the tropical central and eastern Pacific for the peak monsoon season.

PC1 is significantly correlated with OLR over the tropical southeastern Indian Ocean (SEIO), but it does not have significant correlations with OLR over the Arabian Sea and the Bay of Bengal. Because of low OLR values indicating strong convection, the warm SST anomalies in the SEIO are accompanied by significant enhanced convection (negative OLR anomalies), while the warm SST in the Arabian Sea and the Bay of Bengal is generally accompanied by insignificant convection anomalies (Fig. 6). The baroclinic model simulation results indicate that the heating over either the IS or the TP can affect circulation over the Arabian Sea and the Bay of Bengal. Thus, the warm SST anomalies over these regions are more likely forced by atmospheric anomalies. However, the warm SST in the SEIO may be a forcing because it is associated with significant enhanced convection.

To investigate the possible role of tropical SEIO SST in the out-of-phase rainfall variation over the TP and IS, we define the SEIO index (SEIOI) as SST averaged over the tropical SEIO (10°S–0°, 90°–110°E). Figure 7 shows patterns of anomalous rainfall and winds related to Niño-3.4 and SEIOI. Consistent with previous studies, ENSO reduces rainfall in the IS significantly, but not over the central IS as defined in this study, where insignificant rainfall anomalies are observed (Figs. 7a,b). ENSO also does not exert a significant impact on rainfall in the SETP. In contrast, a positive SEIOI is associated with below-normal rainfall in the monsoon zone and a small portion of northwestern IS but above-normal rainfall in the SETP.

ENSO is not accompanied by significant circulation anomalies over the IS at the lower troposphere, whereas it is associated with an anomalous cyclone to the northwest of the IS in the upper troposphere (Figs. 7a,b), which causes convergence over the IS (figures not

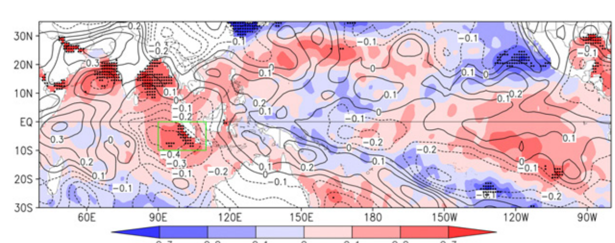

FIG. 6. Patterns of regression of SST (K; shading) on the PC1 and correlation of the PC1 with and OLR (contours; 1974–2007). The green box denotes the region where SST is used to construct the tropical SEIO (10°S–0°, 90°–110°E) SST index; stippling indicates the value of the shading exceeding 95% confidence level.

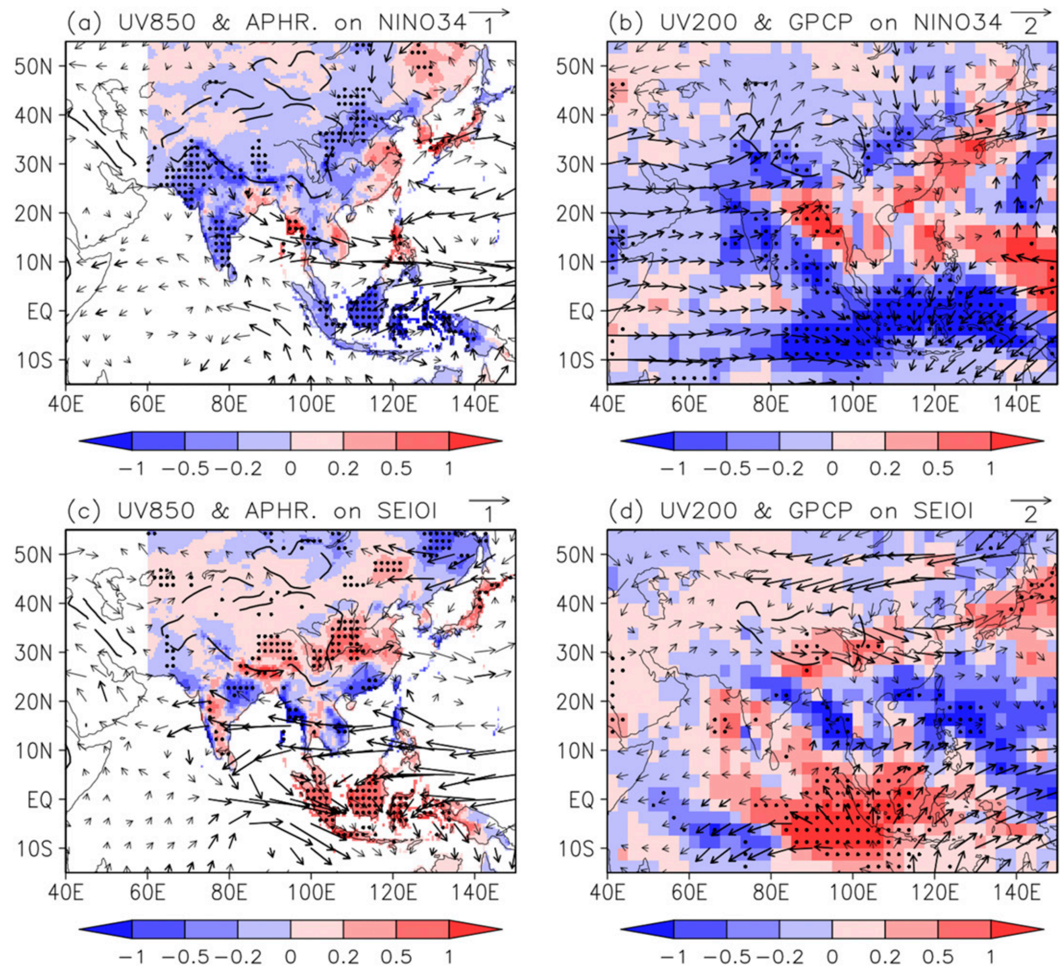

FIG. 7. (a) Patterns of regression of 850-hPa winds (m s^{-1}; vectors) and APHRODITE rainfall (mm day^{-1}; shading) on simultaneous Niño-3.4. (b) Patterns of regression of 200-hPa winds (m s^{-1}; vectors) and GPCP rainfall (mm day^{-1}; shading, 1979–2007) on simultaneous Niño-3.4. (c),(d) As in (a),(b), but Niño-3.4 is replaced by the tropical SEIOI. Stippling indicates the value of the shading exceeding 95% confidence level; thick arrows indicate values exceeding 95% confidence level in either the zonal or the meridional component; the black dashed lines denote the topographic height of 1500 m in (a) and (c) and 3000 m in (b) and (d). Winds at 850 (200) hPa with speed lower than 0.1 (0.2) m s^{-1} are omitted.

shown). This feature is consistent with previous studies showing that ENSO suppresses IS rainfall by causing upper-tropospheric descending motion (e.g., Kumar et al. 2006). In contrast, a positive SEIOI is associated with significant anticyclonic circulation anomalies from the eastern IS to the Philippine Sea in the lower troposphere, resembling that associated with PC1 (Fig. 2c).

The above analyses indicate that the SEIO SST anomalies may cause the dipole rainfall pattern through the following processes. The warm SST anomalies in SEIO could enhance local convection and subsequently induce the lower-tropospheric anomalous cyclone over the eastern Indian Ocean and divergent flow in the upper troposphere (Figs. 7c and 7d, respectively; Gill 1980). Jiang et al. (2016) reported that the enhanced convection over the eastern Indian Ocean and western Maritime Continent can suppress convection from the central IS to the northern Bay of Bengal by strengthening the local Hadley circulation. The suppressed convection over central IS and Bay of Bengal could further excite the anomalous anticyclonic circulation over the central IS to the northern Bay of Bengal, which transports more water vapor into the SETP and favors more rainfall there.

These processes that warm SST anomalies in the SEIO affect the dipole rainfall pattern are produced by the Community Atmosphere Model, version 5.0 (developed by the National Center for Atmospheric Research; Neale et al. 2010). The model simulation results indicated that an increase in SST by 0.5°C in 7.5°S–5°N, 85°–115°E, which is roughly the region with warm SST related to PC1 (Fig. 6), can excite many features related to the PC1 (see Fig. 11 in Jiang et al. 2016), including the dipole rainfall pattern, anomalous anticyclonic circulation from the IS to the Philippine Sea, and even the two upper-tropospheric anomalous cyclones over the midlatitudes. Therefore, the warm SST over the SEIO may be able to excite the dipole rainfall pattern.

Comparison of rainfall patterns related to PC1 and the SEIO SST indicate that warm SEIO anomalies are not associated with significant rainfall decreases over most of the northwestern IS and the upper-tropospheric wave train related to PC1, whereas they are associated with significant rainfall decreases over the eastern-central IS and increases over the SETP. On the other hand, the baroclinic model simulations indicate that the diabatic heating over the SETP could suppress rainfall mostly in the northern IS. Thus, the year-to-year variation of SST in the SEIO only contributes partially to the dipole pattern directly; local interaction of rainfall anomalies between the SETP and central and northern IS may amplify the remote forcing and further strengthen the dipole pattern.

6. Relationship between the dipole pattern, Silk Road wave train, and ENSO

As discussed in the above section, the warm SEIO is not accompanied by a significant rainfall anomaly over most of the northwestern IS and the upper-tropospheric wave train associated with the dipole pattern. Previous studies indicated that the Silk Road wave train may interact with rainfall anomalies over the northwestern IS (e.g., Ding and Wang 2005). Here, we discuss the possible relationship of the Silk Road wave train and the dipole pattern.

Figure 8 shows the rainfall and 200-hPa winds regressed onto the principal component of the first EOF mode of July–August mean meridional winds over 30°–50°N, 30°–130°E, which is used to represent the Silk Road wave train in previous studies (e.g., Kosaka et al. 2012; Orsolini et al. 2015). A positive phase of the Silk Road wave train features anticyclones with centers at 90° and 120°E, respectively, as well as a weak cyclone between them. It is accompanied by above-normal rainfall over the central and northwestern IS but below-normal rainfall over the central and eastern TP. The Silk Road wave train is negatively and significantly correlated with the dipole pattern, with a correlation coefficient of −0.58. Because rainfall over these two regions is highly correlated, we also computed the partial regression of 200-hPa winds and rainfall on SETPR and CISR (Figs. 8b and 8c, respectively). After

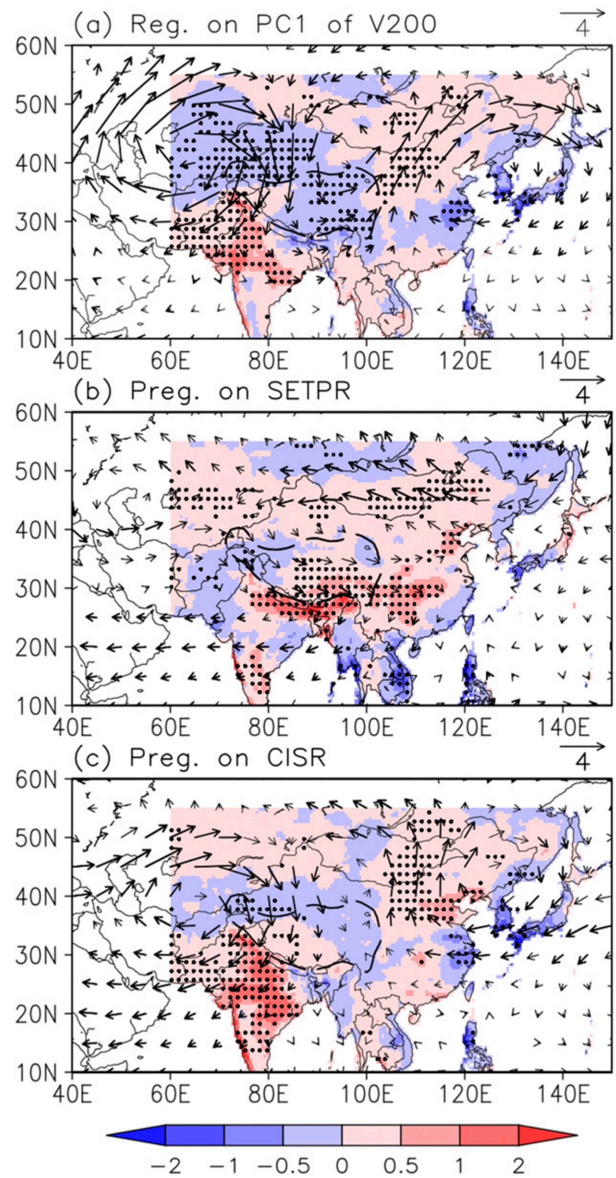

FIG. 8. Patterns of regression of APHRODITE rainfall (mm day^{-1}; shading) and 200-hPa winds (m s^{-1}; vectors) on the PC1 of an EOF analysis applied to anomalous 200-hPa winds over 30°–50°N, 30°–130°E. (b),(c) As in (a), but for partial regression on SETPR and CISR, respectively. Stippling indicates the values exceeding 95% confidence level for rainfall and thick arrows indicate values exceeding 95% confidence level in either the zonal or the meridional component.

removing the effect of CISR, SETPR is not accompanied by the Silk Road wave train; instead, it is accompanied by two anticyclones, located to the west of the TP and over southeastern Siberia, and two cyclones, located over the Caspian Sea and to the northeast of the TP. On the other hand, the CISR-related 200-hPa wind pattern shows the Silk Road wave train in the midlatitudes. The coefficients of correlation between the Silk Road wave train and the SETPR and CISR are 0.56 and −0.28. After removing the effects of each other, the coefficients of correlation between the Silk Road wave train and the SETPR and CISR are 0.50 and 0.05, respectively. Thus, the connection between the Silk Road wave train and the dipole pattern is mostly ascribed to its connection to rainfall over the northwestern IS. It is interesting that increasing rainfall over both the TP and the IS is accompanied by a large anticyclone to the west, consistent with the baroclinic model simulations (Figs. 4b,d).

The relationship between the Silk Road wave train and rainfall over northwestern IS and the underlying processes have been investigated by previous studies (e.g., Ding and Wang 2005; Krishnan et al. 2009), most of which support that the Silk Road wave train and rainfall anomalies over northwestern IS interacts with each other. Some previous studies found that the origin of the Silk Road wave train lies in the internal dry dynamics (e.g., Yasui and Watanabe 2010). On the one hand, when the Silk Road wave train has an anomalous cyclone with center to the east of the Caspian Sea, the westerly anomalies south of the anomalous cyclone tend to advect cold and dry air to the northwestern IS, which could inhibit convective instability and result in less rainfall there (Krishnan et al. 2009). On the other hand, the anomalous decrease in monsoon convection tends to reinforce the Silk Road wave train by exciting Rossby wave dispersion in the subtropical westerlies and shift the Tibetan anticyclone eastward during monsoon breaks (Krishnan et al. 2009). As rainfall anomalies over the central and northern IS can suppress rainfall anomalies over the SETP, the Silk Road pattern may also contribute to the dipole pattern by affecting rainfall over northwestern IS.

As shown in Fig. 6, PC1 is positively correlated with SST in both the SEIO and the tropical central and eastern Pacific. Because of interactions between the tropical Pacific and the tropical Indian Ocean, the SEIOI is significantly and negatively correlated with Niño-3.4 on interannual time scale, with a correlation coefficient of −0.35. To further illustrate the independent effects of SEIO SST and ENSO, we calculated partial regression of rainfall and winds on Niño-3.4 and SEIOI (figures not shown). There are no apparent differences in spatial patterns between the regressions and the partial regressions despite considerable difference in magnitudes in some areas.

The correlations and partial correlations of the PC1, SETPR, and CISR with SEIOI and Niño-3.4 are listed in Table 1. The correlations of SEIO SST with PC1 and CISR get stronger after removing the effects of ENSO. On the other hand, the correlations of ENSO with PC1 and CISR also get stronger after removing the effects of SEIO SST. However, the considerable correlation between ENSO and PC1 does not mean it can cause the dipole pattern, because it is almost uncorrelated with rainfall over the SETP.

TABLE 1. Coefficients of correlation of PC1, the SETPR index, and the CISR index with Niño-3.4 and the SEIOI. All the indices have interdecadal variation removed before being used to calculate correlation. Values in parentheses are coefficients of partial correlation. Values in italic and boldface fonts exceed the confidence levels of 95% and 99%, respectively.

	PC1	SETPR	CISR
Niño-3.4	0.12 (*0.26*)	−0.19 (−0.07)	−0.20 (*−0.29*)
SEIOI	*0.31* (**0.38**)	**0.36** (*0.32*)	−0.19 (*−0.29*)

7. Summary

The TP has been regarded as a key driver for formation and variations of the Indian monsoon. On the other hand, recent studies indicated that the Indian monsoon also exerts a considerable effect on variations of rainfall over the TP. Therefore, the Indian monsoon and the TP should be considered as an interactive system. In this study, we take the Indian monsoon and the TP as a coupled system and investigate its rainfall variation on interannual time scale.

Interannual variations of rainfall across the TP and the IS exhibit a significant dipole pattern. Rainfall in the central and northern IS varies out of phase with rainfall in the SETP, including the main body and the southern slopes. This dipole rainfall pattern is associated with anomalous anticyclones over the IS and the Bay of Bengal, which play an important role in the formation of the dipole rainfall pattern. On the one hand, it transports more water vapor to the SETP and favors more rainfall; on the other hand, it reduces water vapor entering the northern IS and thus suppresses rainfall.

Rainfall anomalies in the SETP and the IS could suppress rainfall to one another by changes in regional circulation due to latent heating of rainfall anomalies. Latent heating over the SETP excites upper-tropospheric descending motion over the northern IS and low-level westerlies to the south, which reduces water vapor entering the northern IS from the Bay of Bengal, favoring below-normal rainfall in the northern IS. On the other hand, latent heating over the central and northern IS could suppress rainfall over the SETP by exciting upper-tropospheric descending motion over the region.

It was shown that the SST anomalies in the SEIO could trigger the dipole rainfall pattern. The enhanced convection over the SEIO due to local warm SST anomalies can suppress convection over the central IS and the northern Bay of Bengal by strengthening the local Hadley circulation. The suppressed convection further induces a local anomalous anticyclone, which transports more water vapor to the SETP and thus favors more rainfall there.

The SEIO SST anomalies are only significantly and negatively correlated with rainfall over the eastern-central IS and a small part of northwestern IS. However, warm SST anomalies in the SEIO are accompanied by a significant increase in rainfall over the SETP, which could suppress rainfall mostly in the northern IS. The Silk Road wave train is also significantly correlated with the dipole pattern because it is interacted with rainfall anomalies over the northwestern IS. Thus, the dipole rainfall pattern is caused by both remote forcings and local interactions.

The correlations between SST and rainfall for both the TP and the IS are lower than the correlation of rainfall between the central and northern IS and the SETP. Interannual variation of rainfall over the IS is also governed by intraseasonal oscillation (e.g., Goswami and Ajayamohan 2001). Our study indicates that atmospheric intraseasonal oscillation also contributes to the dipole rainfall pattern, which will be presented in a separate study.

Observational data analyses and model simulations in this study indicate that the latent heating over the SETP favors an establishment of monsoonal westerlies over the IS, especially the north. However, the strong westerlies cause less rainfall over the northern IS, because water vapor entering the northern IS mainly comes from the Bay of Bengal located to the east. This feature is also produced by a high-resolution regional model (Wang et al. 2016). Thus, the different impacts of TP heating on low-level atmospheric circulation and rainfall over the northern IS should be considered in discussing the influence of the TP on the Indian monsoon.

Acknowledgments. This study was jointly supported by the National Natural Science Foundation of China (Grants 91337107, 91337215, 41661144019, and 41375081), the key operational program for prediction of CMA (CMAHX20160504), and the Basic Research and Operation Program of the CMA Institute of Plateau Meteorology (BROP 201514). MT is partially supported by the National Science Foundation Grant AGS-1607348 and Office of Naval Research MURI Grant 511 N00014-12-1-0911.

REFERENCES

Adler, R. F., and Coauthors, 2003: The Version-2 Global Precipitation Climatology Project (GPCP) monthly precipitation analysis (1979–present). *J. Hydrometeor.*, **4**, 1147–1167, https://doi.org/10.1175/1525-7541(2003)004<1147:TVGPCP>2.0.CO;2.

Ashok, K., Z. Guan, and T. Yamagata, 2001: Impact of the Indian Ocean dipole on the relationship between the Indian monsoon rainfall and ENSO. *Geophys. Res. Lett.*, **28**, 4499–4502, doi:10.1029/2001GL013294.

Bansod, S., Z.-Y. Yin, Z. Lin, and X. Zhang, 2003: Thermal field over Tibetan Plateau and Indian summer monsoon rainfall. *Int. J. Climatol.*, **23**, 1589–1605, doi:10.1002/joc.953.

Behera, S. K., and T. Yamagata, 2003: Influence of the Indian Ocean dipole on the Southern Oscillation. *J. Meteor. Soc. Japan*, **81**, 169–177, doi:10.2151/jmsj.81.169.

Boos, W. R., and Z. M. Kuang, 2010: Dominant control of the South Asian monsoon by orographic insulation versus plateau heating. *Nature*, **463**, 218–222, doi:10.1038/nature08707.

——, and ——, 2013: Sensitivity of the South Asian monsoon to elevated and non-elevated heating. *Sci. Rep.*, **3**, 1192, doi:10.1038/srep01192.

Chen, B., X. Xu, S. Yang, and W. Zhang, 2012: On the origin and destination of atmospheric moisture and air mass over the Tibetan Plateau. *Theor. Appl. Climatol.*, **110**, 423–435, doi:10.1007/s00704-012-0641-y.

Day, A. J., I. Fung, and C. Risi, 2015: Coupling of South and East Asian monsoon precipitation in July–August. *J. Climate*, **28**, 4330–4356, doi:10.1175/JCLI-D-14-00393.1.

Dee, D. P., and Coauthors, 2011: The ERA-Interim reanalysis: Configuration and performance of the data assimilation system. *Quart. J. Roy. Meteor. Soc.*, **137**, 553–597, doi:10.1002/qj.828.

Ding, Q., and B. Wang, 2005: Circumglobal teleconnection in the Northern Hemisphere summer. *J. Climate*, **18**, 3483–3505, doi:10.1175/JCLI3473.1.

Dong, W., and Coauthors, 2016: Summer rainfall over the southwestern Tibetan Plateau controlled by deep convection over the Indian subcontinent. *Nat. Commun.*, **7**, 10925, doi:10.1038/ncomms10925.

Feng, L., and T. Zhou, 2012: Water vapor transport for summer rainfall over the Tibetan Plateau: Multidata set analysis. *J. Geophys. Res.*, **117**, D20114, doi:10.1029/2011JD017012.

Gadgil, S., 2003: The Indian monsoon and its variability. *Annu. Rev. Earth Planet. Sci.*, **31**, 429–467, doi:10.1146/annurev.earth.31.100901.141251.

——, and K. Rupa Kumar, 2006: The Asian monsoon—Agriculture and economy. *The Asian Monsoon*, B. Wang, Ed., Praxis, 651–683.

Gill, A. E., 1980: Some simple solutions for heat-induced tropical circulations. *Quart. J. Roy. Meteor. Soc.*, **106**, 447–462, doi:10.1002/qj.49710644905.

Goswami, B. N., and R. S. Ajaya Mohan, 2001: Intraseasonal oscillations and interannual variability of the Indian summer monsoon. *J. Climate*, **14**, 1180–1198, doi:10.1175/1520-0442(2001)014<1180:IOAIVO>2.0.CO;2.

Hu, Z.-Z., R. Wu, J. L. Kinter, and S. Yang, 2005: Connection of summer rainfall variations in South and East Asia: Role of El Niño–Southern Oscillation. *Int. J. Climatol.*, **25**, 1279–1289, doi:10.1002/joc.1159.

Jiang, X., Y. Li, S. Yang, K. Yang, and J. Chen, 2016: Interannual variation of summer atmospheric heat source over the Tibetan Plateau and the role of convection around the western Maritime Continent. *J. Climate*, **29**, 121–138, doi:10.1175/JCLI-D-15-0181.1.

Kalnay, E., and Coauthors, 1996: The NCEP/NCAR 40-Year Reanalysis Project. *Bull. Amer. Meteor. Soc.*, **77**, 437–471, doi:10.1175/1520-0477(1996)077<0437:TNYRP>2.0.CO;2.

Kosaka, Y., J. S. Chowdary, S.-P. Xie, Y.-M. Min, and J.-Y. Lee, 2012: Limitations of seasonal predictability for summer climate over East Asia and the northwestern Pacific. *J. Climate*, **25**, 7574–7589, doi:10.1175/JCLI-D-12-00009.1.

Krishnan, R., V. Kumar, M. Sugi, and J. Yoshimura, 2009: Internal feedbacks from monsoon–midlatitude interactions during droughts in the Indian summer monsoon. *J. Atmos. Sci.*, **66**, 553–578, doi:10.1175/2008JAS2723.1.

Kumar, K. K., B. Rajagopalan, and M. A. Cane, 1999: On the weakening relationship between the Indian monsoon and ENSO. *Science*, **284**, 2156–2159, doi:10.1126/science.284.5423.2156.

——, ——, M. Hoerling, G. Bates, and M. A. Cane, 2006: Unraveling the mystery of Indian monsoon failure during El Niño. *Science*, **314**, 115–119, doi:10.1126/science.1131152.

Li, C., and M. Yanai, 1996: The onset and interannual variability of the Asian summer monsoon in relation to land–sea thermal contrast. *J. Climate*, **9**, 358–375, doi:10.1175/1520-0442(1996)009<0358:TOAIVO>2.0.CO;2.

Liebmann, B., and C. A. Smith, 1996: Description of a complete (interpolated) outgoing longwave radiation dataset. *Bull. Amer. Meteor. Soc.*, **77**, 1275–1277.

Liu, X., and Z.-Y. Yin, 2001: Spatial and temporal variation of summer rainfall over the eastern Tibetan Plateau and the North Atlantic Oscillation. *J. Climate*, **14**, 2896–2909, doi:10.1175/1520-0442(2001)014<2896:SATVOS>2.0.CO;2.

Mishra, V., B. V. Smoliak, D. P. Lettenmaier, and J. M. Wallace, 2012: A prominent pattern of year-to-year variability in Indian summer monsoon rainfall. *Proc. Natl. Acad. Sci. USA*, **109**, 7213–7217, doi:10.1073/pnas.1119150109.

Neale, R. B., and Coauthors, 2010: Description of the NCAR Community Atmosphere Model (CAM5.0). NCAR Tech. Note NCAR/TN-486+STR, 268 pp., www.cesm.ucar.edu/models/cesm1.1/cam/docs/description/cam5_desc.pdf.

Orsolini, Y. J., L. Zhang, D. H. W. Peters, K. Fraedrich, X. Zhu, A. Schneidereit, and B. van den Hurk, 2015: Extreme precipitation events over north China in August 2010 and their link to eastward-propagating wave-trains across Eurasia: Observations and monthly forecasting. *Quart. J. Roy. Meteor. Soc.*, **141**, 3097–3105, doi:10.1002/qj.2594.

Qiu, J., 2013: Monsoon melee. *Science*, **340**, 1400–1401, doi:10.1126/science.340.6139.1400.

Rajagopalan, B., and P. Molnar, 2013: Signatures of Tibetan Plateau heating on Indian summer monsoon rainfall variability. *J. Geophys. Res Atmos.*, **118**, 1170–1178, doi:10.1002/jgrd.50124.

Rayner, N. A., D. E. Parker, E. B. Horton, C. K. Folland, L. V. Alexander, D. P. Rowell, E. C. Kent, and A. Kaplan, 2003: Global analyses of sea surface temperature, sea ice, and night marine air temperature since the late nineteenth century. *J. Geophys. Res.*, **108**, 4407, doi:10.1029/2002JD002670.

Ting, M., and L. Yu, 1998: Steady response to tropical heating in wavy linear and nonlinear baroclinic models. *J. Atmos. Sci.*, **55**, 3565–3582, doi:10.1175/1520-0469(1998)055<3565:SRTTHI>2.0.CO;2.

Wallace, J. M., and D. S. Gutzler, 1981: Teleconnections in the geopotential height field during the Northern Hemisphere winter. *Mon. Wea. Rev.*, **109**, 784–812, doi:10.1175/1520-0493(1981)109<0784:TITGHF>2.0.CO;2.

Wang, B., B. Xiang, J. Li, P. J. Webster, M. N. Rajeevan, J. Liu, and K.-J. Ha, 2015: Rethinking Indian monsoon rainfall prediction in the context of recent global warming. *Nat. Commun.*, **6**, 7154, doi:10.1038/ncomms8154.

Wang, Z.-Q., A. Duan, M.-S. Li, and B. He, 2016: Influences of thermal forcing over the slope/platform of the Tibetan Plateau on Asian summer monsoon: Numerical studies with the WRF model (in Chinese). *Chin. J. Geophys.*, **59**, 3175–3187, doi:10.6038/cjg20160904.

Wei, W., R. Zhang, M. Wen, X. Rong, and T. Li, 2014: Impact of Indian summer monsoon on the South Asian high and its influence on summer rainfall over China. *Climate Dyn.*, **43**, 1257–1269, doi:10.1007/s00382-013-1938-y.

Wu, G., and Coauthors, 2007: The influence of mechanical and thermal forcing by the Tibetan Plateau on Asian climate. *J. Hydrometeor.*, **8**, 770–789, doi:10.1175/JHM609.1.

——, Y. Liu, B. He, Q. Bao, A. Duan, and F.-F. Jin, 2012: Thermal controls on the Asian summer monsoon. *Sci. Rep.*, **2**, 404, doi:10.1038/srep00404.

Wu, Z., J. Li, Z. Jiang, and T. Ma, 2012: Modulation of the Tibetan Plateau snow cover on the ENSO teleconnections: From the East Asian summer monsoon perspective. *J. Climate*, **25**, 2481–2489, doi:10.1175/JCLI-D-11-00135.1.

Xu, X., C. Lu, X. Shi, and S. Gao, 2008: World water tower: An atmospheric perspective. *Geophys. Res. Lett.*, **35**, L20815, doi:10.1029/2008GL035867.

Yanai, M., C. Li, and Z. Song, 1992: Seasonal heating of the Tibetan Plateau and its effects on the evolution of the Asian summer monsoon. *J. Meteor. Soc. Japan*, **70**, 319–351, doi:10.2151/jmsj1965.70.1B_319.

Yang, K., X. Guo, J. He, J. Qin, and T. Koike, 2011: On the climatology and trend of the atmospheric heat source over the Tibetan Plateau: An experiments-supported revisit. *J. Climate*, **24**, 1525–1541, doi:10.1175/2010JCLI3848.1.

Yao, T., and Coauthors, 2013: A review of climatic controls on $\delta^{18}O$ in precipitation over the Tibetan Plateau: Observations and simulations. *Rev. Geophys.*, **51**, 525–548, doi:10.1002/rog.20023.

Yasui, S., and M. Watanabe, 2010: Forcing processes of the summertime circumglobal teleconnection pattern in a dry AGCM. *J. Climate*, **23**, 2093–2114, doi:10.1175/2009JCLI3323.1.

Yatagai, A., K. Kamiguchi, O. Arakawa, A. Hamada, N. Yasutomi, and A. Kitoh, 2012: APHRODITE: Constructing a long-term daily gridded rainfall dataset for Asia based on a dense network of rain gauges. *Bull. Amer. Meteor. Soc.*, **93**, 1401–1415, doi:10.1175/BAMS-D-11-00122.1.

Zhao, P., and L. Chen, 2001: Climatic features of atmospheric heat source/sink over the Qinghai-Xizang Plateau in 35 years and its relation to rainfall in China. *Sci. China*, **44**, 858–864, doi:10.1007/BF02907098.

Zhou, L., H. Zou, S. Ma, F. Li, J. Zhu, P. Li, and Y. Zhang, 2015: The observed impacts of South Asian summer monsoon on the local atmosphere and the near-surface turbulent heat exchange over the southeast Tibet. *J. Geophys. Res. Atmos.*, **120**, 11 509–11 518, doi:10.1002/2014JD022928.